Hydrodynamics of confined membranes

N. Gov,* A. G. Zilman, and S. Safran
Department of Materials and Interfaces, The Weizmann Institute of Science, P.O.B. 26, Rehovot, Israel 76100
(Received 23 October 2003; revised manuscript received 3 May 2004; published 27 July 2004)

We calculate the hydrodynamic interaction $\Lambda(k)$ (Oseen interaction kernel) and relaxation frequency $\omega(k)$ for the fluctuations of a membrane that is harmonically bounded to a permeable or impermeable wall. We show that due to the confining wall there is an increase in the effective viscosity of the fluid surrounding the membrane. This has been observed in experiments on confined membranes, such as lamellar phases and the red-blood cell membrane. Our results allow a quantitative analysis of these experiments, in terms of the strength of the membrane confining potential and dislocations.

DOI: 10.1103/PhysRevE.70.011104 PACS number(s): 83.10.−y, 47.10.+g, 87.16.−b, 87.19.Tt

I. INTRODUCTION

The dynamic response of confined liquid membranes is important for the understanding of shear flow [1,2] and microrheology [3] experiments on lamellar phases and in the context of biological membranes [4,5]. In the former case, lamellar phases exhibit a rich phase diagram that depends on the spatial conformation of defects in response to shear. A quantitative relation between the unusually large measured effective viscosities and the detailed structure of the membranes in the lamellar phase [1,2], has not been achieved so far. Biological membranes in cells are spatially confined by the cytoskeleton [4], and therefore also exhibit dynamics which is different from that of a free bilayer.

In this paper we first calculate the dynamics of a fluctuating, but overall stationary, confined fluid membrane (a similar calculation has been carried out before [6,7]). The result presented here, aside from the derivation of the dynamics, is the definition of an effective viscosity η_{eff} of the membrane-fluid system. This effective viscosity can be larger than that of a free fluid, due to the confinement of the fluid and the deviation of the membranes from flatness, i.e., their normal undulations. The maximal value of η_{eff} is given by the ratio of d/ξ, where d is the normal confinement of the membrane, and ξ is the mean distance in the plane of the membrane, between membrane-wall collisions (or membrane-membrane collisions in the case of lamellar stack) due to thermal wandering. The expressions we derive for the hydrodynamic (Oseen) interaction of the membrane, through the surrounding fluid, show hydrodynamic screening at long wavelengths, due to the wall. We define an effective viscosity for the flow of the surrounding fluid due to the membrane undulations. The largest amplitude undulations, at the persistence length of the membrane, require transport of the surrounding fluid and cause the measured viscosity of the system to differ from that of the free fluid. We argue that the maximal value of our effective viscosity, which occurs at this wavelength, gives the measured effective viscosity of sheared confined membranes. This definition of effective viscosity is the main result of this paper.

We then use this definition to analyze the results of relaxation experiments of red-blood cells (RBC) [5]. We further apply our definition of η_{eff}, which we calculate for an overall stationary but thermally fluctuating membrane, to the case of sheared lamellar stacks. In these experiments [1–3] we attribute the anomalous increase in the measured viscosity to the advection of confined fluid over and between colliding membranes which now flow relative to each other rather than fluctuate thermally. The membranes in the stack are assumed to have the static undulating form allowed by the lamellar confinement and the preexisting defects, while their dynamics relative to each other is driven by the shear flow. When the stack is sheared, these undulations move with respect to each other and collide (Fig. 1), resulting in fluid and membrane flows in the normal (z) direction. These normal fluid flows around, and due to, the membrane undulations are responsible for the anomalously large measured viscosity. Our calculations therefore allow a quantitative analysis of the experiments on lamellar L_α phases under shear [1,2], other microrheology measurements [3], and analysis of the fluctuations of membranes of the red-blood cell (RBC) [5]. In the former case, we can relate the observed "shear thickening" and "shear thinning" (increase and reduction in the viscosity with increasing shear rate, respectively) to the changes in the

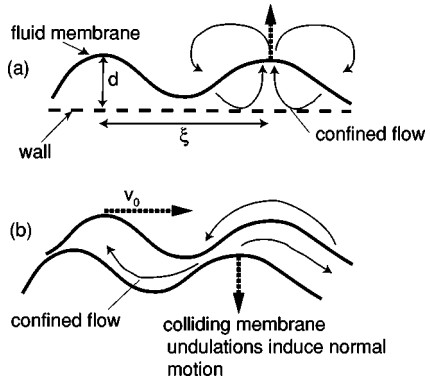

FIG. 1. An illustration of the confined fluid dynamics around an (a) overall-stationary but thermally fluctuating membrane near a wall, compared to (b) a sheared stack of membranes with undulations that collide. The shear rate $\dot{\gamma}=v_0/d$ gives the relative velocity v_0 between the membranes.

*Current address: Department of Chemical Physics, The Weizmann Institute of Science, P.O.B. 26, Rehovot, Israel 76100.

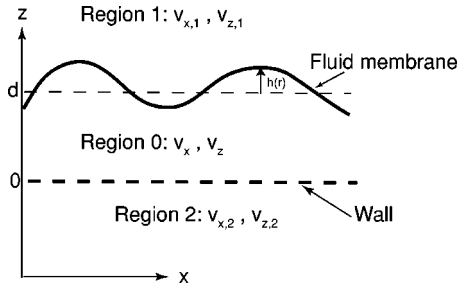

FIG. 2. An illustration of the domain of the solution of the Navier-Stokes equations (1)–(5), [(A1)–(A20)] for the motion of a membrane bounded to a permeable or impermeable wall.

number of defects per membrane. In the latter example, the RBC has a layer of water that is effectively trapped between its outer membrane and the cytoskeleton [4], giving rise to the large effective measured viscosity.

II. MODEL

We describe here the model and the results, deferring the detailed calculations to the Appendix.

We solve the Navier-Stokes equations for the normal fluctuations of a membrane that is confined by an impermeable or a permeable wall [6,8] (Fig. 2). The actual bilayer-wall interactions that keep the membrane at the constant average separation, d, from the wall, are not explicitly described, and are taken into account through a uniform binding harmonic potential. The membrane is assumed to be flat on average, with small fluctuations of amplitude h, at an equilibrium distance d from the flat wall (Fig. 2). The rest of the space is filled with an incompressible viscous fluid, of density ρ and viscosity η. The hydrodynamic variables in the region of fluid trapped between the membrane and the wall have no subscript (Fig. 2), while the hydrodynamic variables in the semi-infinite regions above the membrane and below the wall have subscripts 1 and 2, respectively.

The Stokes equations of motion for a viscous fluid are [9] (see Fig. 2)

$$\rho\frac{\partial v_x}{\partial t} = -\frac{\partial p}{\partial x} + \eta\frac{\partial^2 v_x}{\partial x^2} + \eta\frac{\partial^2 v_x}{\partial z^2}$$

$$\rho\frac{\partial v_z}{\partial t} = -\frac{\partial p}{\partial z} + \eta\frac{\partial^2 v_z}{\partial x^2} + \eta\frac{\partial^2 v_z}{\partial z^2} \tag{1}$$

(we assume that the system is uniform and stationary with respect to the y direction: $v_y=0$), with the additional constraint of incompressibility

$$\frac{\partial v_x}{\partial x} = -\frac{\partial v_z}{\partial z}. \tag{2}$$

We are interested in small amplitude normal (z-direction) fluctuations, h, of the membrane from its flat position $h=0$ (Fig. 2). The fluctuations in the flow field can therefore be written in terms of the wave vector k_x. Finally, the boundary conditions have to be specified. The normal velocity of the fluid on both sides of the membrane is the same, and is equal to the normal velocity of the membrane $v_m=\partial h/\partial t$. Additionally, we require that the shear stress is the same on both sides of the membrane [10]: $\sigma'_{xz}(0)=\sigma'_{xz,1}(0)$, where the shear stress is defined by [9]

$$\sigma'_{xz} \equiv \eta\left(\frac{\partial v_x}{\partial z} + \frac{\partial v_z}{\partial x}\right). \tag{3}$$

The boundary conditions for the fluid at the wall are the following: for the impermeable case they are no slip, so that $v_x(d)=v_z(d)=0$. For the case of a permeable wall we use Darcy's law for the permeation of the z component of the fluid velocity, and no-slip boundary condition for the x-component at the wall

$$v_z(d) = v_{z,2}(d) = \lambda\ \delta p(d), \tag{4}$$

$$v_x(d) = v_{x,2}(d) = 0, \tag{5}$$

where $\delta p(d)$ is the pressure difference across the permeable wall, $\lambda=L_p/\eta$, and λ is the permeability of the wall [8]. The length L_p gives the radius of imaginary holes in the permeable wall, such that the fluid velocity inside the holes changes from zero at the inner surface of the hole to $v_z(d)$ at their centers.

Solving the resulting equations [Eqs. (1) and (2)] for the three variables v_x, v_z, and p (see the Appendix), we calculate the pressure difference and viscous stress tensor along the z direction, in each region and at the membrane. This gives us an expression for the force acting in the $\hat{z}$ direction on the membrane due to the surrounding fluid flow. The Oseen interaction kernel, $\Lambda(|\boldsymbol{r}-\boldsymbol{r}'|)$, is defined by the relation between the velocity of the membrane and the force which we just calculated due to the fluid motion [Eq. (A16)]

$$v_m = \frac{\partial h(\mathbf{r},t)}{\partial t} = -\int d^2r'\,\Lambda(|\boldsymbol{r}-\boldsymbol{r}'|)F_z(\boldsymbol{r}',t). \tag{6}$$

After a Fourier transform and an expansion in k_z to first order in the small inertial term $\omega\rho/\eta$ (A3), we find for an impermeable wall

$$\Lambda(k_x) = -\frac{1}{4\eta k_x}[e^{-2dk_x}(1 - e^{2dk_x} + 2dk_x + 2(dk_x)^2)], \tag{7}$$

compared with $\Lambda_{free}(k_x)=1/4\eta k_x$, which is the Oseen interaction for a free membrane [11–13]. In Fig. 3 we plot the function Λ/Λ_{free}, which indeed shows the free-membrane behavior in the limit $k_x\to\infty$ or $d\to\infty$, and completely screened interactions in the limit $k_x\to 0$, where we get: $\Lambda/\Lambda_{free}\to d^3k_x^3/3$.

To derive the relaxation frequency of the membrane fluctuations, we note that in equilibrium, the force due to the surrounding fluid is balanced [15] by the force due to the intrinsic bending energy of the membrane [13,16]

$$h_{k_x}\omega(k_x) = \Lambda(k_x)\frac{\partial H_{bend}}{\partial h_{k_x}}, \tag{8}$$

where H_{bend} is the bending energy of the membrane, which is written in terms of the small normal displacement h

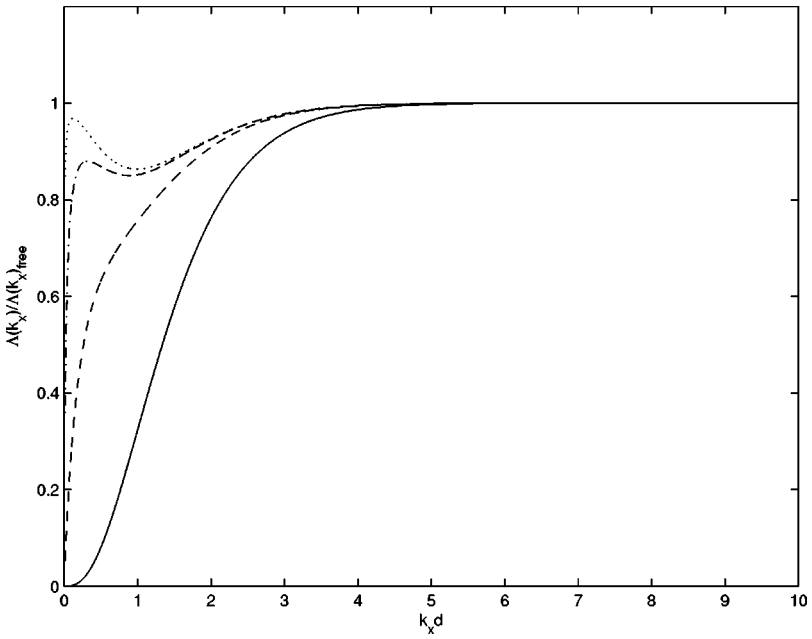

FIG. 3. The function $\Lambda(k_x)/\Lambda_{free}(k_x)$. Solid line: impermeable wall [Eq. (7)]; dash: $L_p=d$; dash-dot: $L_p=10d$; dot: $L_p=100d$ [Eq. (12)].

$$H=\frac{1}{2}\int d^2r[\kappa(\nabla^2h(r))^2+\gamma h(r)^2], \tag{9}$$

where κ is the intrinsic curvature modulus and γ is the strength of a uniform harmonic potential. We neglect here any surface tension terms, since we deal with an infinite fluid membrane. We also neglect terms proportional to Gaussian curvature, which is similar to spontaneous curvature terms that are here neglected [6,16]. Furthermore, the Gaussian curvature is a topological constant, so that small fluctuations that do not change the membrane topology (i.e., no holes), do not excite this term.

The presence of the harmonic potential γ imposes a finite average amplitude of the membrane thermal fluctuations, d_T, at the value of the separation from the wall d [16]

$$d_T^2=d^2=\langle h(0)h(0)\rangle=\frac{k_BT}{8\sqrt{\kappa\gamma}}. \tag{10}$$

The choice of harmonic potential for description of the confinement is natural when the physical situation provides a "soft" substrate: For the RBC case the harmonic potential is natural since the cytoskeleton is made up of soft filaments (spectrin) that are linked to form a soft shell on which the bilayer sits [4]. Similarly for lamellar phases (see the next section), the spacing d is determined by thermal and structural fluctuations of neighboring membranes. This also produces a soft restoring force. For the hard wall case this harmonic approximation is good for small amplitude fluctuations, where large area membrane-wall contacts are unlikely. In any realistic scenario the membrane is held at a constant spacing d from the wall by some (unspecified) contacts, which we here do not describe. These contacts, even when of small area and sparse (such as in the RBC [4,14]), will likely induce a real harmonic-like potential. Hard-wall-membrane collisions are therefore rare, and will be neglected.

The relaxation frequency ω is therefore finally given by

$$\omega(k_x)=[\kappa k_x^4+\gamma]\Lambda(k_x). \tag{11}$$

In the limit of short length scales ($k_x\to\infty$), we recover the free-membrane behavior $\omega\to\kappa k_x^3/4\eta$. In the limit of long length scales the dynamics are now modified, $\omega\to\gamma d^3k_x^2/3\eta$, so the response is "stiffer" than that of a free membrane, with the rigid wall providing an effectively stronger restoring force due to the transport of the confined water over length scales $1/k_x$. At intermediate wavelengths $q_0\ll q\ll 1/d$ [where $q_0=(\gamma/\kappa)^{1/4}=1/\xi$ and ξ is the persistence length of the membrane], we recover the result of Brochard

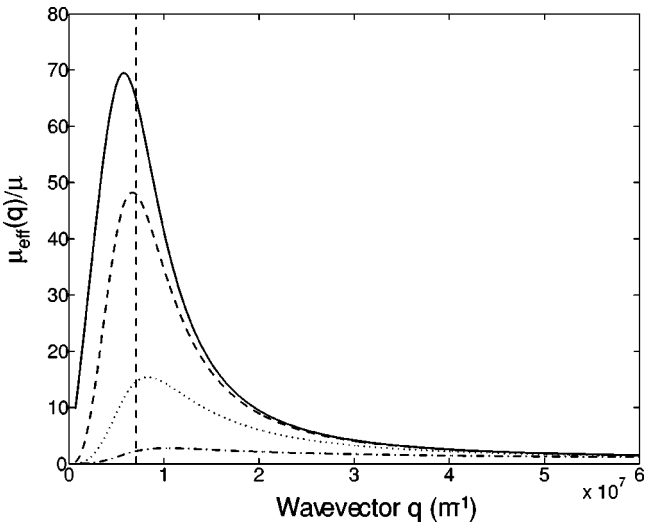

FIG. 4. The function $\eta_{eff}(q)/\eta$ as a function of the wave vector q, using the elastic and confinement parameters of the RBC [4] (see Sec. IV). Solid line: impermeable wall [Eq. (14)]; dash: $L_p=0.1$ nm; dot: $L_p=1$ nm; dash-dot: $L_p=10$ nm. Vertical dashed line indicates the persistence length of the confined membrane q_0.

et al. [15]: $\omega \to \kappa k_x^6 d^3/3\eta$. This last regime is in fact the most relevant for most measurements, as we find below. The importance of the persistent length ξ is in the fact that the height-height correlation function saturates at this length scale [16], so that the curvature modes of longer lengths do not contribute. In other words, it gives the scale of the largest thermal modes that are correlated. Longer wavelengths conform to the confining potential and are not thermally correlated (screening effect).

For a permeable wall we get

$$\Lambda_{perm}(k_x) = \frac{1}{4k_x\eta}\frac{e^{-2dk_x}(1 - e^{2dk_x}(1 + 4L_p k_x) + 2dk_x + 2(dk_x)^2(1 + 2L_p k_x))}{1 + 4L_p k_x}. \tag{12}$$

In the limit of impermeable wall $L_p \to 0$ we recover the previous result (7).

In Fig. 3 we plot the function $\Lambda_{perm}(k_x)/\Lambda_{free}(k_x)$, which shows free-membrane behavior in the limit $k_x \to \infty$, and screened interactions in the limit $k_x \to 0$, where we now have $\Lambda_{perm}(k_x)/\Lambda_{free}(k_x) \to 4L_p k_x$.

III. EFFECTIVE VISCOSITY

In the previous section, we calculated the effects of confinement on the membrane dynamics. We saw that confinement of the fluid flow around the membrane results in significant modification of the relaxation frequency (11). We begin with deriving a working definition of the effective viscosity of the confined membrane, and then apply this to various physical realizations of confined membranes in the next section.

First, we calculate the rate of dissipation of energy due to membrane fluctuations of wave vector k

$$\dot{E} = \left\langle f\frac{\partial h_k}{\partial t}\right\rangle = \langle -h_k[\kappa k^4 + \gamma]\omega_k h_k\rangle = \omega_k k_B T, \tag{13}$$

where for convenience we use the notation $k_x = k$, the force $f = \partial H_{bend}/\partial h_k$ as in (8), and $\langle h_k^2\rangle = k_B T/[\kappa k^4 + \gamma]$ [16]. We use the equal time correlations $h_k(t)h_k(t)$, so we can use the equilibrium value of $\langle h_k^2\rangle$. We see that the rate of energy dissipation is inversely proportional to the bare fluid viscosity, since $\omega_k \propto 1/\eta$ [see Eqs. (7) and (11)]. The result of Eq. (13), $\omega_k \propto 1/\eta$, is a general one for thermal flows [17]. For the specific case of fluctuating membrane, we have a fixed amplitude of thermal fluctuations $\sim d$ by Eq. (10), as is the energy dissipated per membrane fluctuation ($k_B T$), while the rate of fluctuations is slowed down by the viscosity, thereby reducing $\dot{\gamma}$, and with it $\dot{E}$.

It is convenient to express the modified dynamics of a confined membrane, through the following definition of an effective viscosity η_{eff}. We define this effective viscosity by comparing the rate of energy dissipation Eq. (13) in confined and unconfined membranes, i.e., the ratio of the frequencies

$$\eta_{eff}(k)/\eta = \frac{\omega_{free}}{\omega} = -\frac{\kappa k^4 e^{2dk}}{(1 - e^{2dk} + 2dk + 2(dk)^2)(\gamma + \kappa k^4)}, \tag{14}$$

where $\omega_{free} = (\kappa k^4)/4k\eta_{eff}(k)$. In other words, the effective viscosity $\eta_{eff}(k)$ transforms the rate of energy dissipation of a free membrane to that of a confined membrane. A similar expression follows for the case of a permeable wall, using the result of Eq. (12) instead of (7) in Eqs. (11) and (14). The results are shown in Fig. 4.

In the limit of long length scales ($k \to 0$), this expression Eq. (14) is linear in the wave vector: $\eta_{eff}(k)/\eta \to 3\kappa k/(4\gamma d^3)$ (Fig. 4). Specifically, in this limit, the confined effective viscosity is much smaller than that of a free membrane, due to the faster oscillation frequency $\omega \simeq \gamma d^3 k^2/3\eta \gg \kappa k^3/4\eta$. The confinement forces the membrane to adopt a nearly flat, lamellar nature at long wavelengths, where no normal (z-direction) motion persists. This is the "lubrication" approximation regime for the flow of thin, flat films [16]. In the opposite limit of short length scales, we recover the free viscosity of the surrounding fluid and $\eta_{eff}(k)/\eta \to 1$ (Fig. 4). Our definition provides a natural measure of the departure of the membrane from a flat state, as one can see by noting that in the limit $k \to 0$ the membrane is flat due to the confinement, while in the limit $k \to \infty$, the membrane is flat due to its own bending stiffness. Indeed, in these limits $\eta_{eff}(k)/\eta$ is either unity or small. It is only in the intermediate regime, as we'll see later, that $\eta_{eff}(k)/\eta$ can attain large values, signaling a strong deviation from flatness.

Note that the above definition of $\eta_{eff}(k)/\eta$ [Eq. (14)] is independent of the temperature, which is the driving force for the thermal fluctuations. The reason for this is that both confined and free membranes are driven by the same thermal power. The fluid flow and amount of energy dissipated, at each wave vector k, is determined by the amplitude of the fluctuations, which is clearly different for the free and confined case [16]. As seen in Fig. 4, as the permeation increases (increasing L_p) the effective viscosity approaches that of unconfined membrane, that is $\eta_{eff}(k)/\eta \to 1$. Only at long wavelengths, where the z component of the motion is suppressed, does the confinement still affect the membrane dynamics.

The confined membrane has maximal thermal fluctuations at the persistence length $\xi=1/q_0$. At these intermediate wavelengths $q_0 \ll q \ll 1/d$, where $\omega \to \kappa k^6 d^3/3\eta$, we get $\eta_{eff}(k)/\eta \to 3/4(dk)^3$, which in general can be larger than unity. This means that at these wavelengths the response of the confined membrane is significantly slower than that of the free membrane; this implies a larger effective viscosity of the surrounding medium. Indeed, at the characteristic wave vector q_0, the viscosity ratio of Eq. (14) has its peak value (Fig. 4)

$$\eta_{eff}/\eta \simeq -\frac{e^{2dq_0}}{(-2+2e^{2dq_0}-4dq_0-4(dq_0)^2)}. \tag{15}$$

We are going to use this maximal viscosity η_{eff}/η (15) as the measured effective viscosity of sheared confined membranes when we analyze experimental data in the next section. The motivation for this definition is as follows: At the wave vector, q_0, we compare our definition of $\eta_{eff}(k)/\eta$ [Eq. (14)] arising from Eq. (13), and the expressions for the dissipation rate in a sheared fluid [9]

$$\dot{E} = \frac{\eta}{2}\int dV\left(\frac{\partial v}{\partial z}\right)^2 = \frac{\eta L^2 v_0^2}{2d}, \tag{16}$$

where L is the lateral size of the slab of sheared flow, and the shear rate across the intermembrane spacing of width d is given by $\dot{\gamma}=v_0/d$. The local average velocity due to thermal fluctuation is estimated by $v_0 \simeq d\omega_k$, and the lateral size of the slab of flow at this wave vector is $L \sim \xi$, which we substitute in Eq. (16)

$$\dot{E} = \frac{\eta_{eff}\xi^2\omega_k^2 d^2}{2d} = \frac{\eta_{eff}}{16\sqrt{2}}\xi^2\frac{\sqrt{k_BT}}{(\kappa\gamma)^{1/4}}\frac{\kappa k^3}{4\eta_{eff}}\omega_k$$
$$\simeq \omega_k k_B T (k\xi)^3\frac{\sqrt{\kappa/k_BT}}{16\sqrt{2}} \sim \omega_k k_B T, \tag{17}$$

where we used $d^2=k_BT/8\sqrt{\kappa\gamma}$ [Eq. (10)] and $(k\xi)^3=1$ for $k=q_0$, and $\sqrt{\kappa/k_BT}/16\sqrt{2}\sim 1/8$. Beginning with the standard definition of shear flow, Eq. (16), we roughly recover the result of Eq. (13) for the thermally fluctuating membrane. The main point is that the equilibrium amplitude of thermal fluctuations d^2 is proportional to k_bT and determines the energy dissipated per mode k. The effective viscosity, defined in Eq. (14), is thus consistent (up to an order of magnitude) with the usual "shear flow" definition of Eq. (16), for the maximal value of the viscosity at wavelengths of the order of the persistence length. We therefore identify the measured effective viscosities, with the maximal calculated effective viscosity of a membrane fluctuation at the wave vector q_0 [as in Eq. (15)], where the deviation from flatness (amplitude of fluctuations) is largest.

In the limit of weak harmonic confinement, $dq_0 \ll 1$, the maximal effective viscosity of Eq. (15) diverges as $\eta_{eff}/\eta \to 3/8(dq_0)^3$. We can rewrite this expression in terms of the amplitude of thermal fluctuations of the membrane, d_T, which is given by the harmonic confinement γ [Eq. (10)] [16], so that in general we find

$$\eta_{eff}/\eta = 3\sqrt{8}\left(\frac{\kappa}{k_BT}\right)^{3/2}\left(\frac{d_T}{d}\right)^3, \tag{18}$$

which is $\sim 15-500(d_T/d)^3$ for typical lipid bilayers (where $\kappa \sim 1-10k_BT$). If the membranes are indeed confined to have undulations whose amplitude does not exceed the distance d, as for the rigid wall we presented above, then we have $d_T=d$. In general, the confinement of the membrane fluctuation amplitude can be constrained by a stronger harmonic potential γ, so that the membrane shows fluctuations whose amplitudes are less than d ($d_T<d$). This results in a lower effective viscosity, as seen in Eq. (18). Alternatively, a weaker confinement, with $d_T>d$, can also occur, as we discuss below.

Our definition of the effective viscosity of membrane fluctuations is related to the measured viscosity in sheared lamellar phases as follows: If the membranes were perfectly flat, the measured viscosity of the sheared stack would be that of the free fluid $\eta_{eff}/\eta=1$. However, the membranes in thermal equilibrium are not flat; they have an undulating form constrained by the lamellar confinement and preexisting defects. When the stack is sheared, these undulations move with respect to each other and collide (Fig. 1), resulting in fluid and membrane flows in the normal (z) direction. These normal fluid flows around, and due to, the membrane undulations are responsible for the anomalously large measured viscosity [1–3] (Fig. 1) in lamellar stacks of membrane, typically of the order $\eta_{eff}/\eta \sim 10^3-10^2$. The additional energy dissipation due to the collision-induced membrane oscillations normal to the flow, in the confinement of the neighboring membranes, therefore increases the observed viscosity. When the sheared membranes collide and are pushed sideways (see also Fig. 1), the resulting local flow field is similar to the confined normal fluctuations we calculated in the previous section. Our calculation predicts the rate of dissipation that such an undulation produces in Eq. (13), albeit for an overall stationary (i.e., not flowing) and unsheared membrane.

IV. PHYSICAL REALIZATIONS OF CONFINED MEMBRANES

An important biological example where the confinement of the liquid membrane affects its dynamics is in the red-blood cell (RBC) [4]. In this composite lamellar structure, there is a two-dimensional cytoskeleton network that is attached to and therefore confines the thermal fluctuations of the outer lipid membrane. We have previously shown [4] that the cytoskeleton network acts like a rigid shell at a constant average separation, d, from the liquid membrane. At the frequencies of the thermal fluctuations, this shell turns out to be impermeable [4,18]. In addition to the confinement of the thermal fluctuation spectrum, the rigid shell also increases the effective viscosity of the water layer that is trapped between the cytoskeleton and the bilayer, by constraining its flow.

For this case of the RBC we have the following typical values: $d \sim 30$ nm and $\gamma \sim 5\times 10^7$ J/m^4 [4], which, according to Eq. (14), gives a maximum effective viscosity (18) of

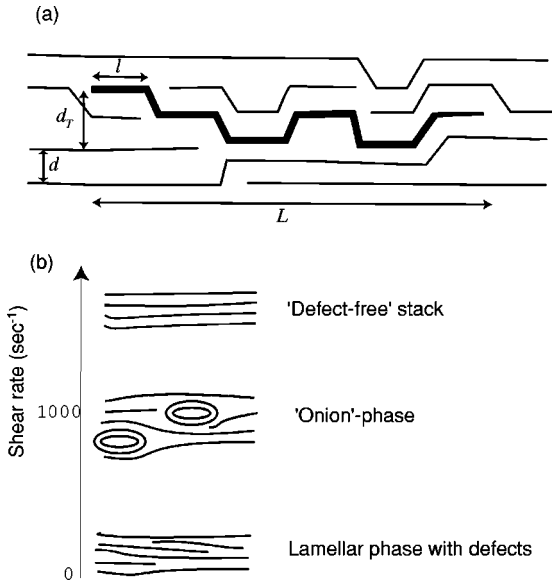

FIG. 5. (a) A schematic example of a lamellar phase of membranes with average separation d, showing defects that produce finite membrane segments L, with edge dislocations every distance l. (b) A schematic phase diagram of lamellar membranes as a function of shear rate, as observed in experiments [1,2].

$\eta_{eff}/\eta \sim 70$ (Fig. 4). This value is in close agreement with the value $\approx 50-100$ deduced from the measured relaxation times of a deformed RBC [5]. In these experiments, the cytoplasm flows along the cytoskeleton mesh, as the deformed RBC relaxes back to its undeformed structure. Thus, an almost impermeable cytoskeletal shell, separated at a fixed distance from the bilayer [4], results in the significantly larger effective viscosity required to fit these dynamical experiments. Another biological example of a flowing membrane confined by a cytoskeleton is the extraction of tether from neuronal growth cones [19]. In this system the water behaves as if it is trapped in a thin layer (~ 1 nm) between the membrane and the underlying actin mesh, resulting in an extraordinarily large value of the effective viscosity.

For an infinite stack of membranes in an L_α lamellar phase (Fig. 5), the confinement of each bilayer is not by a rigid wall, but due to the steric repulsion of the neighboring membranes (except for the outer ones that are confined by the rigid walls of the channel) [1]. The bulk modulus of this phase is given by Ref. [16]: $B=36(k_BT)^2/\pi^2\kappa d^4$, which corresponds to the parameter γ in Eq. (18). The resulting maximal effective viscosity (taking $\kappa \sim 10k_BT$) is $\eta_{eff}/\eta \sim 3$. This number is typical of the measured viscosity of a defect-free lamellar phase [1–3,21]. By "defect-free" we mean a lamellar phase where dislocations and multilayered vesicles are absent.

We suggest that the effective viscosity of lamellar phases with defects can be treated as follows: Defects in the lamellar stacking are typically dislocation lines that allow membranes to "penetrate" through their neighbors [1,12,20] (Fig. 5). The layer of confined water around each membrane is still $\sim d$ thick, while the effective static confinement parameter γ is now smaller, allowing for the membrane to have undulations with an average amplitude $d(T) > d$. This is typical of a lamellar phase at low shear rates [1–3] [Fig. 5(b)]. The measured effective viscosity in these systems is typically of the order $\eta_{eff}/\eta \sim 10^3$. Values of this order of magnitude are predicted by our theory, if the membranes are allowed to have thermal fluctuations with an amplitude of $d_T/d \sim 2-3$ (depending on the ratio κ/k_BT) in Eq. (18), due to the strong nonlinear dependence of η_{eff}/η on the ratio d_T/d. We therefore treat the dynamics of a lamellar phase with defects as a lamellar phase with an effectively smaller static confinement γ, that results in a value of $d(T)/d > 1$. By making this choice we assume that the fluid flow over the membrane undulations is still confined within a layer of thickness d (the average intermembrane separation) with respect to the membrane, so that our calculation is still valid (Fig. 5). The large effective viscosity is therefore attributed to the slow fluid flow through this thin layer, while it is periodically blocked by the large membrane undulations, which now exceed d. This is a very rough description of the rather complicated dynamics of the entangled membranes, though it is useful in allowing us to make predictions concerning the density of defects and the shear-rate dependence of the effective viscosity. Since the fluid is mostly confined to a layer of thickness d around the membrane, except at the defect sites themselves, this may be a reasonable starting point to describe this complicated system. Our treatment supposes that the viscosity is dominated by the solvent-bilayer flow, and not by movement ("creep") of the defects inside the membranes [20]. The transition from lamellar to multilayered vesicles (MLV) [1] is not described by our model, which allows for an analysis of the measured viscosity at each geometry separately.

If the membranes meander through the defects in the stack in a random walk (Fig. 5), then the ratio d_T/d is given by $\sqrt{L/l}$, where L is the average size of a membrane segment, and l is the average distance between defects along the membrane segment, so that $n_d = l/L$ is the dimensionless density of defects. In experiments [2,3], it seems that at low shear rates the lamellar phase [Fig. 5(b)] has membrane segments of average length $L \sim 10d$. The measured effective viscosity of $\eta_{eff}/\eta \sim 10^3$ therefore suggests that at low shear rates the density of defects is maximal, with $l \sim d$, so that $d_T/d \simeq \sqrt{L/l} \sim 3$. As the shear rate increases, the membranes in the stack become more ordered and the dislocations are removed, until a defect-free lamellar phase [1–3] forms at high shear rates [Fig. 5(b)]. As the density of defects decreases, so does the effective viscosity: $\eta_{eff}/\eta \propto n_d^{-3/2}$ [using Eq. (18)].

We can further compare our analysis above with the results of experiments on the time-dependent behavior of a lyotropic lamellar phase under shear flow [22,23]. In these experiments [23] it was found that the phase of onions can oscillate between a disordered and ordered (triangular) packing state, with a corresponding change in the shear rate (for a constant stress). These periodic rearrangements of the onions are limited by the rate at which the trapped water confined between the onions can flow out (Fig. 6). We treat the onions as rigid bodies which only change their packing from ordered to disordered, which is reasonable since the onions are quite small and compact, as described in Refs. [22,23]. From simple geometry, the shape of the trapped water between the onions has an average width of $d \sim 0.155R$. Using our results

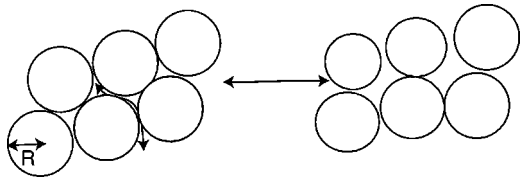

FIG. 6. Time-dependent dynamics of onion phase [23]. The oscillations are between the ordered-triangular (left) and disordered (right) packing of the onions. These are limited by the flow of the water into and out of the confined spaces between the onions, when these roll over each other.

so far, we write the frequency of these oscillations as $\omega = \kappa q^3/4\eta_{eff}$, where $q \sim 1/R \sim 0.5\ \mu\mathrm{m}^{-1}$, $\kappa \sim k_B T$, and $\eta_{eff}/\eta \sim (R/d)^3 \simeq 250$. We therefore recover the measured [23] frequency of $\sim$1000 s. In this analysis we treat fluid flows on the length scale of the radius R or smaller, as essentially those we calculated for flat confined membranes. This is a reasonable approximation for the dynamics of the whole onions.

Furthermore, since we predict that the effective viscosity will not depend on the size of the onions, the frequency should depend on the radius through $\omega \propto R^{-3}$. This relation naturally explains the measured dependence of the frequency on the temperature (Fig. 6 of Ref. [23]), as it follows from the observed temperature dependence of the radius (in the relevant range of shear rates; see Fig. 5 of Ref. [22]); the radius is found to increase by a factor of $\sim$1.5 when the temperature increases from 23.5°C to 27.8°C. This corresponds to a decrease of the frequency by a factor of $1.5^3 - 3.3$ over this range of temperatures, in good agreement with the observed data [23]. Similar slow dynamics appears in a sheared sponge phase [24], where periodic transitions between large and small multilamellar droplets occur.

Recent experiments on adsorbed lipid membranes [25] show the dynamic implications of confinement on membrane fluctuations. In these experiments the membranes are layered and form adhesion patches, with trapped "blisters" of water in between. The adhesion of the membranes confines the thermal fluctuations to patches of lateral size $L \sim 0.44\ \mu$m, with a root-mean-square fluctuation amplitude of $d \sim 6.5$ nm. When the relaxation rate of these fluctuations was measured, it was found to be two orders of magnitude slower than expected for a free membrane. If we use the amplitude d as the typical thickness of the water layer in which the membrane is free to fluctuate in our expression for the impermeable wall [Eq. (11)], we find a time scale of $\sim$1 s for the dynamics at the measured wave vector $q \simeq 2.3\ \mu\mathrm{m}^{-1}$. This is in excellent agreement with the measured value of $\sim$0.9 s.

Another example of recent experiments where enhanced effective viscosity has been observed is the rheological study of giant vesicles by a micropipette [26]. In these experiments the shear-induced reduction in the amplitude of thermal fluctuations was measured by the suction of the vesicle into a micropipette. The critical time scale of the vesicle fluctuations that are affected (diminished) by the shear was found to be $\tau_0 \sim 140$ s, which is $\sim$180 times larger than the slowest vesicle membrane mode: $\tau_{vesicle} = \eta R_0^3/\kappa$, where $R_0 \simeq 20\ \mu$m

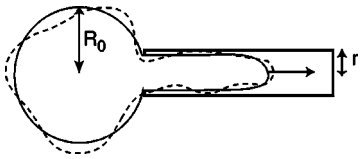

FIG. 7. Dynamics of a vesicle (solid line) drawn into a micropipette (thick rectangle) in the experiments of Ref. [26]. The free fluctuations of wavelength $\sim R_0$ have the largest amplitude (dashed line), and are confined into the micropipette of radius r, limiting the dynamics.

is the vesicle radius and $\kappa \simeq 22 k_B T$ [26]. These slowest modes have the longest wavelength (R_0) and largest amplitude, so that they present the largest obstacle when the vesicle is being drawn into the micropipette (of radius $r \sim 5\ \mu$m; Fig. 7). From our discussion so far, the effective viscosity these fluctuations encounter inside the micropipette is enhanced by a factor of (15): $\sim (R_0/r)^3 \sim 100$ (taking $q_0 \sim 1/R_0$). Note that the confinement inside a cylindrical micropipette is higher than in the slab geometry we calculated above. This setup can be used to systematically check our predicted relation between the effective viscosity η_{eff}/η [Eq. (15)], and the ratio $\sim (R_0/r)$.

V. CONCLUSIONS

In this paper we have calculated the hydrodynamics of fluctuations in confined fluid membranes. We find that the effects of confinement dramatically modify the dynamics of the membranes. We introduce a new definition for the effective viscosity of a confined membrane, which we relate to the observed effective viscosities in various physical realizations of confined membranes such as lamellar phases and in red-blood cell. These results can also help in the analysis of dynamical phase transitions occurring in lamellar membranes under shear flow. In particular, they allow one to make a quantitative connection between the geometric conformation of the membranes, their defects, and the measured effective viscosity.

ACKNOWLEDGMENTS

This work was supported by an ISF grant and by the BSF Grant Number 183-2002. The authors are grateful to the donors of the Petroleum Research Fund administered by the American Chemical Society and the Schmidt Minerva Center for their support. N.G.'s research is being supported by the Koshland Postdoctoral Fellowship.

APPENDIX: SOLUTION OF STOKES EQUATIONS

The equations of motion for the fluid are (1) and (2). We next make a standard Fourier transform, by taking the x dependence to be given by $\exp(-ik_x x)$. The incompressibility condition [Eq. (2)] is therefore: $v_x = (-i/k_x)\,\partial v_z/\partial z$. From this set of equations the pressure is given by

$$p = -\frac{1}{k_x^2}\left[k_z^2\frac{\partial v_z}{\partial z} - \frac{\partial^3 v_z}{\partial z^3}\right]. \tag{A1}$$

Substituting for the z- and t dependence an exponential form $\exp(\pm k_z z - \omega t)$, we have an equation for k_z

$$\frac{k_z^2}{k_x^2}[-\rho\omega + \eta(k_x^2 - k_z^2)] = -\rho\omega + \eta(k_x^2 - k_z^2), \tag{A2}$$

which has the solutions

$$k_z^2 = \begin{cases} k_x^2 \\ k_x^2 - \rho\omega/\eta. \end{cases} \tag{A3}$$

From now on we shall use k_z to mean the second solution. The fluid velocity fields are therefore given by

$$v_z = e^{-\omega t - ik_x x}(Ae^{-k_x z} + Be^{-k_z z} + Ce^{k_x z} + De^{k_z z}),$$

$$v_{z,1} = e^{-\omega t - ik_x x}(A_1 e^{k_x z} + B_1 e^{k_z z}),$$

$$v_{z,2} = e^{-\omega t - ik_x x}(A_2 e^{-k_x z} + B_2 e^{-k_z z}), \tag{A4}$$

with the corresponding x components given by the incompressibility condition

$$v_x = \frac{-i}{k_x}e^{-\omega t - ik_x x}(-k_x Ae^{-k_x z} - k_z Be^{-k_z z} + k_x Ce^{k_x z} + k_z De^{k_z z}),$$

$$v_{x,1} = \frac{-i}{k_x}e^{-\omega t - ik_x x}(k_x A_1 e^{k_x z} + k_z B_1 e^{k_z z}),$$

$$v_{x,2} = \frac{-i}{k_x}e^{-\omega t - ik_x x}(-k_x A_2 e^{-k_x z} - k_z B_2 e^{-k_z z}). \tag{A5}$$

1. Impermeable wall

For simplicity let us first consider the impermeable wall case, i.e., the region 2 is removed (Fig. 2). The boundary conditions at the membrane are

$$v_z(0) = v_{z,1}(0),$$

$$v_x(0) = v_{x,1}(0),$$

$$\sigma'_{xz}(0) = \sigma'_{xz,1}(0), \tag{A6}$$

where the shear stress is defined in Eq. (3).

First, using the first two boundary conditions of (A6), we get

$$A_1 = \frac{-A\left(1 + \frac{k_z}{k_x}\right) - 2B\frac{k_z}{k_x}}{1 - \frac{k_z}{k_x}} + C,$$

$$B_1 = \frac{2A + B\left(1 + \frac{k_z}{k_x}\right)}{1 - \frac{k_z}{k_x}} + D. \tag{A7}$$

Inserting these into the last boundary condition of (A6), we get

$$B = -A\frac{k_x}{k_z} \Rightarrow A_1 = A + C,\ B_1 = B + D. \tag{A8}$$

The equations we need to solve are for the three independent parameters A, C, D, using the following boundary conditions at the wall (at $z = d$)

$$v_z(d) = 0, \tag{A9}$$

$$v_x(d) = 0. \tag{A10}$$

Combining these two equations with the condition

$$v_z(0) = v_{z,1}(0) = v_m, \tag{A11}$$

where $v_m = \partial h/\partial t$ is the membrane velocity in the z direction, we have a complete set of equations to solve

$$\begin{matrix}\text{Eq.(A11)} \\ \text{Eq.(A9)} \\ \text{Eq.(A10)}\end{matrix} \Rightarrow \begin{pmatrix} 1 - \frac{k_x}{k_z} & 1 & 1 \\ e^{-dk_x} - \frac{k_x}{k_z}e^{-dk_z} & e^{dk_x} & e^{dk_z} \\ k_x(e^{-dk_z} - e^{-dk_x}) & k_x e^{dk_x} & k_z e^{dk_z} \end{pmatrix}\begin{pmatrix} A \\ C \\ D \end{pmatrix} = \begin{pmatrix} v_m \\ 0 \\ 0 \end{pmatrix}. \tag{A12}$$

Using MATHEMATICA [27] we solve for A, C, D

$$\begin{pmatrix} A \\ C \\ D \end{pmatrix} = \begin{pmatrix} 1 - \frac{k_x}{k_z} & 1 & 1 \\ e^{-dk_x} - \frac{k_x}{k_z}e^{-dk_z} & e^{dk_x} & e^{dk_z} \\ k_x(e^{-dk_z} - e^{-dk_x}) & k_x e^{dk_x} & k_z e^{dk_z} \end{pmatrix}^{-1}\begin{pmatrix} v_m \\ 0 \\ 0 \end{pmatrix}. \tag{A13}$$

Substituting the parameters A, C, D in the expression for the pressure (A1), we find at the membrane ($z = 0$) for the two regions

$$p(0) = k_x(A - C)\left(\frac{k_z^2}{k_x^2} - 1\right)$$

$$p_1(0) = -k_x(A+C)\left(\frac{k_z^2}{k_x^2}-1\right)$$

$$\Rightarrow \delta p(0) = p_1(0) - p(0) = -2Ak_x\left(\frac{k_z^2}{k_x^2}-1\right). \tag{A14}$$

The viscous stress tensor along the z direction, at the membrane, is given by

$$\sigma'_{zz} \equiv 2\eta\frac{\partial v_z}{\partial z} \Rightarrow \sigma'_{zz}(0) = \sigma'_{zz,1}(0) = 2(k_xC + k_zD). \tag{A15}$$

The final expression for the force acting in the $+\hat{z}$ direction on the membrane is

$$F_t = F(0) - F_1(0) = -\hat{z}[p(0) - \sigma'_{zz}(0)] + \hat{z}[p_1(0) - \sigma'_{zz,1}(0)]$$
$$= +\hat{z}[p_1(0) - p(0)]. \tag{A16}$$

2. Permeable wall

We now consider the case of a permeable wall. The boundary conditions at the membrane remain unchanged, while at the wall the boundary conditions are first given by the continuity of the velocity fields

$$v_z(d) = v_{z,2}(d)$$

$$v_x(d) = v_{x,2}(d) \tag{A17}$$

Using (A5) and (A17), we find

$$A_2 = A + C\frac{k_xe^{2k_xd}(l_x+k_z)}{k_z-k_x} + 2D\frac{e^{(k_x+k_z)d}k_z}{k_z-k_x},$$

$$B_2 = -A\frac{k_x}{k_z} - C\frac{2k_xe^{(k_x+k_z)d}}{k_z-k_x} - D\frac{e^{2k_zd}(k_x+k_x)}{k_z-k_x}. \tag{A18}$$

The pressure difference at the permeable wall is given by (A1)

$$p(d) = \frac{e^{-dk_x}(A - Ce^{2dk_x})(k_z-k_x)(k_z+k_x)}{k_x}$$

$$p_2(d) = \frac{e^{-dk_x}(k_z+k_x)(A(k_z-k_x) + e^{2dk_x}(2e^{d(k_z-k_x)}Dk_z + C(k_z+k_x)))}{k_x} \Rightarrow \delta p(d) = p(d) - p_2(d) = -2e^{dk_x}\frac{(C + De^{d(k_z-k_x)})k_z(k_x+k_z)}{k_x}. \tag{A19}$$

We next use Darcy's law for the permeation of the z component and the no-slip boundary condition for the x component at the wall, Eqs. (4) and (5). The complete set of equations we have to solve is now [compared to (A12) for the impermeable case]

$$\begin{matrix}\text{Eq. (A11)}\\ \text{Eq. (4)}\\ \text{Eq. (5)}\end{matrix} \Rightarrow \begin{pmatrix} 1-\frac{k_x}{k_z} & 1 & 1 \\ e^{-dk_x} - \frac{k_x}{k_z}e^{-dk_z} & e^{dk_x} + L_p\frac{2e^{dk_x}k_z(k_x+k_z)}{k_x} & e^{dk_z} + L_p\frac{2e^{dk_z}k_z(k_x+k_z)}{k_x} \\ k_x(e^{-dk_z} - e^{-dk_x}) & k_xe^{dk_x} & k_ze^{dk_z} \end{pmatrix}\begin{pmatrix} A \\ C \\ D \end{pmatrix} = \begin{pmatrix} v_m \\ 0 \\ 0 \end{pmatrix}. \tag{A20}$$

Again using MATHEMATICA [27], we solve for A, C, D, to substitute in the expression for the force (A14) and (A16).

[1] D. Roux, F. Nallet, and O. Diat, Europhys. Lett. **24**, 53 (1993); O. Diat, D. Roux, and F. Nallet, Phys. Rev. E **51**, 3296 (1995); J. I. Escalante, M. Gradzielski, H. Hoffmann, and K. Mortensen, Langmuir **16**, 8653 (2000).

[2] A. Léon, D. Bonn, J. Meunier, A. Al-Kahwaji, O. Greffier, and H. Kellay, Phys. Rev. Lett. **84**, 1335 (2000).

[3] D. Mizuno, Y. Kimura, and R. Hayakawa, Phys. Rev. Lett. **87**, 088104 (2001).

[4] N. Gov, A. Zilman, and S. Safran, Phys. Rev. Lett. **90**, 228101 (2003).

[5] M. A. Peterson, Phys. Rev. A **45**, 4116 (1992); H. Engelhardt, H. Gaub, and E. Sackmann, Nature (London) **307**, 378 (1984); E. A. Evans, Methods Enzymol. **173**, 3 (1989).

[6] U. Seifert, Phys. Rev. E **49**, 3124 (1994).

[7] The result in our paper is somewhat different from that of Seifert [6] due to differences in the boundary conditions at the membrane surface: while Seifert uses an "in-plane incompressibility" condition for the fluid near the membrane, which implies (since $v_y=0$) $dv_x/dx=0$, we use a zero-shear-stress condition, which implies that the x-z component of the shear on both sides of the membrane are equal [Eq. (3)]. Since the water near the membrane is a three-dimensional fluid, a two-dimensional incompressibility condition should not be relevant and we have focused on the force balances instead. Our con-

dition [10] assumes that the membrane cannot support shear stress across its width, which is reasonable if the membrane is in the fluid phase. In any case, the differences in the final expressions are not significant as far as the role of the wall is concerned.

[8] J. Prost, J.-B. Manneville, and R. Bruinsma, Eur. Phys. J. B **1**, 465 (1998).

[9] L. D. Landau and E. M. Lifshitz, *Fluid Mechanics* (Pergamon Press, Oxford, 1982).

[10] S. Ramaswamy, J. Prost, W. Cai, and T. C. Lubensky, Europhys. Lett. **23**, 271 (1993).

[11] M. Doi and S. F. Edwards, *The Theory of Polymer Dynamics* (Clarendon, Oxford, 1986).

[12] A. G. Zilman and R. Granek, Eur. Phys. J. B **11**, 593 (1999).

[13] S. W. Marlow and P. D. Olmsted, Phys. Rev. E **66**, 061706 (2002).

[14] N. Gov and S. Safran, Phys. Rev. E **69**, 011101 (2004).

[15] F. Brochard and J. F. Lennon, J. Phys. (France) **36**, 1035 (1975).

[16] S. A. Safran, *Statistical Thermodynamics of Surfaces, Interfaces and Membranes*, Frontiers in Physics Vol. 90 (Addison-Wesley, Reading, MA, 1994).

[17] See, for example, P. M. Chaikin and T. C. Lubensky, *Principles of Condensed Matter Physics* (Cambridge University Press, Cambridge, 1995).

[18] The rapid motion of the flexible spectrin filaments that make up the cytoskeleton cover the holes in the mesh in a time $\sim 2\ \mu$s, which is much shorter than the typical time of the bilayer thermal fluctuations, which have frequencies 1–10 Hz.

[19] R. M. Hochmuth *et al.*, Biophys. J. **70**, 358 (1996).

[20] C. Meyer, S. Asnacios, C. Bourgaux, and M. Kleman, Rheol. Acta **39**, 223 (2000).

[21] M. Mihailescu *et al.*, Phys. Rev. E **66**, 041504 (2002).

[22] P. Sierro and D. Roux, Phys. Rev. Lett. **78**, 1496 (1997).

[23] A. S. Wunenburger, A. Colin, J. Leng, A. Arneodo, and D. Roux, Phys. Rev. Lett. **86**, 1374 (2001); J.-B. Salmon, S. Manneville, and A. Colin (unpublished); e-print cond-mat/0307609.

[24] L. Courbin, P. Panizza, and J.-B. Salmon, Phys. Rev. Lett. **92**, 018305 (2004).

[25] Y. Kaizuka and J. T. Groves (unpublished).

[26] N. Fa, C. M. Marques, E. Mendes, and A. P. Schröder, Phys. Rev. Lett. **92**, 108103 (2004).

[27] MATHEMATICA v. 4.